International Journal of Nanomedicine

Dovepress
open access to scientific and medical research

Open Access Full Text Article

ORIGINAL RESEARCH

Ultrasound Molecular Imaging of Bladder Cancer via Extradomain B Fibronectin-Targeted Biosynthetic GVs

Yanan Feng[1,2,*], Yongsheng Hao[3,*], Yuanyuan Wang[3], Weijian Song[1,4], Shanxin Zhang[1], Dong Ni[5], Fei Yan[3], Litao Sun[1]

[1]Cancer Center, Department of Ultrasound Medicine, Zhejiang Provincial People's Hospital (Affiliated People's Hospital), Hangzhou Medical College, Hangzhou, Zhejiang, 310014, People's Republic of China; [2]Department of Abdominal Ultrasound, The Affiliated Hospital of Qingdao University, Qingdao, Shandong, 266000, People's Republic of China; [3]Center for Cell and Gene Circuit Design, CAS Key Laboratory of Quantitative Engineering Biology, Shenzhen Institute of Synthetic Biology, Shenzhen Institute of Advanced Technology, Chinese Academy of Sciences, Shenzhen, 518055, People's Republic of China; [4]Bengbu Medical College, Bengbu, 233030, People's Republic of China; [5]Medical Ultrasound Image Computing (MUSIC) Laboratory, Shenzhen University, Shenzhen, 518055, People's Republic of China

*These authors contributed equally to this work

Correspondence: Litao Sun; Fei Yan, Tel +86 13946037056, Email litaosun1971@sina.com; fei.yan@siat.ac.cn

Purpose: Ultrasound molecular imaging (UMI) has proven promising to diagnose the onset and progression of diseases such as angiogenesis, inflammation, and thrombosis. However, microbubble-based acoustic probes are confined to intravascular targets due to their relatively large particle size, greatly reducing the application value of UMI, especially for extravascular targets. Extradomain B fibronectin (ED-B FN) is an important glycoprotein associated with tumor genesis and development and highly expressed in many types of tumors. Here, we developed a gas vesicles (GVs)-based nanoscale acoustic probe (ZD2-GVs) through conjugating ZD2 peptides which can specially target to ED-B FN to the biosynthetic GVs.

Materials and Methods: ED-B FN expression was evaluated in normal liver and tumor tissues with immunofluorescence and Western blot. ZD2-GVs were prepared by conjugating ZD2 to the surface of GVs by amide reaction. The inverted microscope was used to analyze the targeted binding capacity of ZD2-GVs to MB49 cells (bladder cancer cell line). The contrast-enhanced imaging features of GVs, non-targeted control GVs (CTR-GVs), and targeted GVs (ZD2-GVs) were compared in three MB49 tumor mice. The penetration ability of ZD2-GVs in tumor tissues was assessed by fluorescence immunohistochemistry. The biosafety of GVs was evaluated by CCK8, blood biochemistry, and HE staining.

Results: Strong ED-B FN expression was observed in tumor tissues while little expression in normal liver tissues. The resulting ZD2-GVs had only 267.73 ± 2.86 nm particle size and exhibited excellent binding capability to the MB49 tumor cells. The in vivo UMI experiments showed that ZD2-GVs produced stronger and longer retention in the BC tumors than that of the non-targeted CTR-GVs and GVs. Fluorescence immunohistochemistry confirmed that ZD2-GVs could penetrate the tumor vascular into the interstitial space of the tumors. Biosafety analysis revealed there was no significant cytotoxicity to these tested mice.

Conclusion: Thus, ZD2-GVs can function as a potential UMI probe for the early diagnosis of bladder cancer.

Keywords: ultrasound contrast agents, gas vesicles, ultrasound molecular imaging, tumor diagnosis

Introduction

In the past decades, the emergence of ultrasound molecular imaging (UMI) has attracted gradually increasing interest due to its capability to assess dynamic changes at the cellular and molecular levels. However, most commonly developed ultrasonic probes are based on the micron-sized (1–10 μm), gas-containing microbubbles that can only remain within the vascular lumen, which limits their application potential in extravascular diseased tissues or cells, such as tumors.[1–3] By contrast, nano-sized bubbles have the advantages over microbubbles, with can penetrate blood vessels and reach the extravascular tissue space, especially for tumors.

Received: 14 March 2023
Accepted: 11 August 2023
Published: 29 August 2023

Graphical Abstract

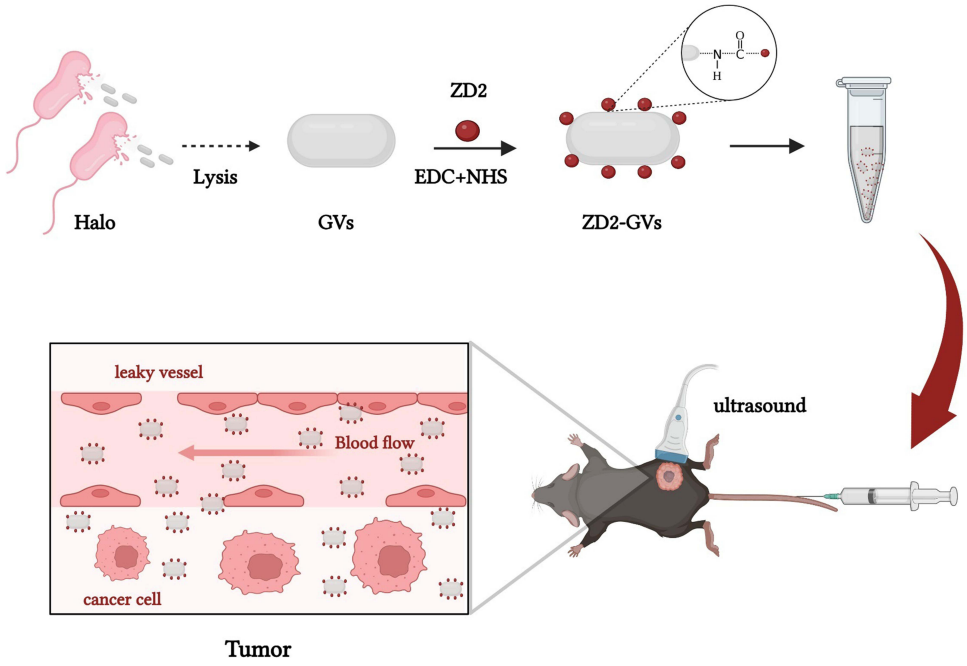

Recently, targeted or non-targeted nanobubbles (NBs) consisting of various phospholipid or polymer shells have been developed for the ultrasound contrast agents.[4] At present, chemically synthesized nanoscale contrast agents have been reported to have good acoustic properties, most of them have particle sizes greater than 500 nm, limiting tumor penetration performance.[5–8] Recently, the nanoscale biosynthetic gas vesicles (GVs) with 200 nm particle size from *Halobacterium NRC-1* (Halo) have been demonstrated excellent ultrasound contrast signals in murine livers and stronger tumor penetration capability for tumors.[9,10] Structurally, GVs have a 2 nm protein shell with hydrophobic inner surfaces and hydrophilic outer surfaces.[11–14] This particular structure allows GVs to permit gas from the surrounding media into the vesicle.[11,15,16] As a result, no pressure gradient exists between the inside and outside of GVs, which makes them physically stable.[15] Similarly, an increasing number of studies show that GVs have great potential for ultrasound imaging and therapeutic applications.

Numerous evidences demonstrated that many tumor extracellular matrix (ECM) proteins closely interact with tumor progression and metastasis.[17–22] One of them, extradomain-B fibronectin (ED-B FN), is considered as the most abundant ECM components involved in tumor neovascularization and significantly upregulated in many invasive cancers, including pancreatic cancer, breast cancer, oral cancer, and prostate cancer.[23–26] It has been reported that ED-B FN can function as a promising target molecular imaging marker due to its preferred upregulation and abundance in tumors.[24] Recently, Han et al developed a cyclic nonapeptide CTVRTSADC (ZD2), which binds to ED-B FN with high specificity.[26] ZD2-based MRI and SPECT imaging probes have been developed and showed its great application value[27–30] in different malignancies, such as oral cancer,[25] breast cancer,[31] pancreatic cancer,[24] and prostate cancer.[26] Here, we reported for the first time the ZD2-modified acoustic probe based on the biosynthetic GVs, referred as ZD2-GVs, and examined its potential to early diagnosis of bladder cancer (BC).

Materials and Methods

Preparation of GVs, CTR-GVs, and ZD2-GVs

Halobacterium NRC-1 (Halo) bacteria were cultured at 37 °C with constant shaking at 220 rpm/min for 7–10 days. GVs were isolated by TMC lysate buffer (10 mM Tris-HCl, 2.5 mM $MgCl_2$, 2 mM $CaCl_2$, and pH 7.5) and centrifuged

for 3 times at 350 g for 4 h. The isolated GVs were washed with phosphate buffered saline (PBS) and purified for 3 times by centrifugation at 250 g for 4 h and finally stored at 4 °C. The concentration of GVs was determined by measuring the optical density at 500 nm (OD_{500}) using a full-wavelength microplate reader (Scientific Multiskan GO, Thermo Fisher, Waltham, MA, USA). The amount of substance used for the subsequent calculation of GVs was calculated according to the methods and data provided by Andrew I Yao,[32] Shapiro MG,[15] and Lakshman A.[33] Fluorescein isothiocyanate (FITC) labeled ZD2 peptide (with amino acid sequence of CTVRTSADC), control peptide (with amino acid sequence of CERAK), and their unlabeled peptides were obtained from Gill Biochemical Company Limited (Shanghai, China). For ZD2-GVs synthesis, ZD2 peptides were conjugated to the protein shells of GVs by N-ethyl-N'-[3-dimethylaminopropyl] carbodiimide/N-hydroxy succinimide (EDC/NHS) cross-linking reaction. Briefly, the solvent of GVs (OD_{500} = 3.0) was replaced with 0.1 M $NaHCO_3$ (pH 8.3). 3 mg EDC, 3 mg NHS and 200 μg ZD2 peptides were added to 1 mL MES buffer (0.1 M MES, 0.5 M NaCl, pH 5.6) and the solution was stirred in 4 °C for 3 h to active the carboxyl group of ZD2. Then, 1 mL of GVs at OD_{500} 3.0 was added dropwise. The reaction mixture was stirred for overnight at 4 °C, followed by centrifugation and rinse for 4–5 times with PBS. The same preparation method was adapted to prepare the control probe GVs modified by CERAK peptides. In addition, FITC labeled peptide was conjugated to the protein shells of GVs, and the fluorescence intensity was determined by the microplate reader to confirm whether it is successful conjugation and calculate the number of peptides conjugated GVs.

Characterization of GVs, CTR-GVs, and ZD2-GVs

According to the method by Lakshmanan et al,[33] GVs solution was diluted and placed on the copper mesh, negatively stained with 2% phosphotungstic acid, and then dried at room temperature. The morphology of GVs was examined by transmission electron microscopy (TEM) (Hitachi H-7650, Hitachi Limited, Tokyo, Japan). In brief, the GVs, CTR-GVs and ZD2-GVs samples were diluted to appropriate concentrations at room temperature. The particle size and zeta potential measurements were performed by Zetasizer analyzer (Zetasizer Nano S90, Malvern, Worcestershire, UK). The measurements were repeated at least three times.

Tumor Immunofluorescence Staining

Studies have shown that ED-B FN is not expressed in normal tissues.[34] Therefore, tumor tissues and normal liver tissues from mice were collected after euthanasia according to IACUC and embedded in OCT, cut by Microtome cryostat (Leica CM1950, Germany) into 5 μm. Tissue sections are blocked in QuickBlock™ blocking buffer for 30 min and stained with the anti-EDB-FN G4 primary monoclonal antibody (Absolute Antibody, Oxford, UK) overnight at 4 °C. Then, secondary Alexa Fluor 488 anti-rabbit antibody (1:1000) was incubated with these sections for 1 h at room temperature. The nuclei were stained by 4'6-diamidino-2-phenylindole (DAPI). The fluorescence images were acquired by an inverted microscope (IX73, Olympus, Tokyo, Japan).

Western Blot

Western blot was used to quantitatively determine the expression of ED-B FN in tumor tissues and normal liver tissues. Firstly, tissues were lysed in RIPA buffer (Beyotime Biotechnology, Shanghai, China) supplemented with PMSF (Beyotime Biotechnology, Shanghai, China). Protein concentration was determined by the BCA protein assay kit. Equal protein from each sample was mixed with 5× sodium dodecyl sulfate-polyacrylamide gel electrophoresis (SDS-PAGE) sample loading buffer (Beyotime Biotechnology, Shanghai, China) and separated by SDS-PAGE on 8% (v/v) resolving gel. The protein was transferred to the Polyvinylidene Fluoride (PVDF) membrane (Beyotime Biotechnology, Shanghai, China). Membranes were blocked with fast blocking and incubated with anti-EDB-FN (G4, Absolute Antibody, Oxford, UK) and anti-β-actin (Beyotime Biotechnology, Shanghai, China) primary antibodies overnight. Membranes were washed and incubated with horseradish peroxidase-conjugated anti-rabbit IgG secondary antibodies (Beyotime Biotechnology, Shanghai, China) for 45 minutes. Membranes were activated with Immobilon Western Chemiluminescent HPR Substrate and imaged with the tanon 5200 chemiluminescent imaging system.

In vitro Binding of ZD2-GVs with Tumor Cells

Mouse bladder cancer cells (MB49), purchased from the American Type Culture Collection, were cultured in Dulbecco's Modified Eagle's Medium (DMEM) supplemented with 10% fetal bovine serum (FBS) and 1% penicillin-streptomycin (PS). The cells were incubated at 37°C in 5% CO_2 with the medium changed every other day. MB49 cells were cultured overnight in 24-well plates (5×10^4 cell per well). After being washed for 3 times with PBS, 100 μL FITC-labeled ZD2-GVs or FITC-labeled CTR-GVs at OD_{500} 3.0 were added to each well and incubated darkly for 5 min at room temperature. Subsequently, the free ZD2-GVs or CTR-GVs were rinsed with PBS for 3–5 times. After that, these cells were fixed with 4% paraformaldehyde (PFA) for 15 min and stained with DAPI. Finally, the cells were examined under an inverted microscope. Competitive inhibition experiment was performed by pre-incubating the cells with unlabeled free ZD2 peptide at room temperature for 30 min, followed by the addition of FITC-labeled ZD2-GVs. Binding of FITC-labeled CTR-GVs on the MB49 cells was examined as a control.

Animal Models

Animal experiments were approved by the Ethics Committee of Shenzhen Institutes of Advanced Technology, Chinese Academy of Sciences (SIAT-IACUC-190522-YGS-YF-A07438), and were performed in strict accordance with the national standards of the People's Republic of China (Laboratory animal: Guideline for ethical review of animal welfare [GB/T 35892-2018], Guideline of assessment for humane endpoints in animal experiment [RB/T 173-2018]). The male C57BL/6 (6 weeks old, body weight 20 ± 1.5 g) were supplied by Beijing Vital River Laboratory Animal Technology Company Limited. All mice were housed on 12:12 light:dark cycle with free access to food and water. MB49 cells (1×10^6 / each mouse) in 100 μL of PBS were injected into the flank of the right leg region. Tumor size was monitored with caliper measurements. After 3 weeks, mice were used for UMI and histological analysis when the tumor size reached an average size of 100 mm^3.

In vitro Ultrasound Imaging

The in vitro imaging phantoms were prepared with 1% agarose in pure water. Different concentrations of GVs, CTR-GVs or ZD2-GVs (OD_{500} = 0.5, 1.0, 1.5, and 2.0) were added into phantom wells, respectively. Imaging was performed using ultrasound diagnostic equipment (Mindray Resona 7, Mindray, Shenzhen, China) with the L11-3U line array transducer (3.0–11.0 MHz). The ultrasonic probe was placed directly one side of the agarose. The parameters were kept as follows: acoustic power: 2.75%, mechanical index: 0.112, contrast gain: 70 db.

In vivo Ultrasound Imaging

During imaging, mice C57BL/6 were anesthetized with 1% isoflurane in oxygen at 2 L/min on a heating pad. GVs, CTR-GVs, or ZD2-GVs (100 μL at OD_{500} 3.0) were injected into mice (n = 3) via the tail vein at random order to minimize bias, and ultrasound imaging was performed using a 3.0–11.0 MHz line array transducer equipped by Mindray Resona 7. All parameters (acoustic power: 5.13%, mechanical index: 0.167, contrast gain: 70 db) remain unchanged during imaging. Images were continuously acquired for 10 min. To minimize any deviations from the two injections in the same mouse, injections were separated by at least 30 min. The contrast signals were quantitatively analyzed using software built in the Mindray Resona 7 device after manually defining the regions of interest (ROI).

Histological Examination

In order to confirm that GVs were able to pass through the endothelial gaps of tumors, the tumor-bearing mice (n = 9) were injected with 100 μL FITC-labeled GVs, FITC-labeled CTR-GVs, or FITC-labeled ZD2-GVs via the caudal vein and then tumors were collected after 10 min and used for frozen sections. The tumor sections were fixed with 4% PFA, and rat anti-mouse CD31 antibodies (Abcam, Cambridge, UK) were added and incubated with overnight at 4 °C, followed by incubation with Cy5-conjugated goat anti-rabbit secondary antibody (Abcam, Cambridge, UK) to visualize the vessels. The cell nuclei were stained with DAPI. Images were recorded using confocal microscope (A1R, Nikon, Japan) and quantified using Image J software.

Biosafety Testing

Cell Counting Kit-8 (CCK-8) was used for determining the viability of cells. Briefly, MB49 cells were cultured in 96-well cell plates (1×10^4 cells per well) and treated with 100 μL GVs (OD_{500} = 0–3.0) for 24 or 48 h. Then, CCK-8 solution was added to the plate and incubated for 1 h. The absorbance was measured at 450 nm. As for the in vivo biosafety, 100 μL PBS, GVs, and ZD2-GVs at OD_{500} 3.0 were intravenously injected into the healthy C57BL/6 mice (n = 3, respectively). After 24 h, the major organs, including heart, liver, spleen, lung, and kidney, were removed for tissue section and H&E staining. Eighteen healthy C57BL/6 mice were selected for hematological experiment. Nine were intravenously injected with 100 μL of ZD2-GVs (OD_{500} = 3.0), and the other nine were injected with 100 μL of PBS as the control. The whole blood and the serum from these mice were collected before injection, on the first day and on the seventh day after injection for blood biochemistry test (Wuhan Servicebio Technology Company, China).

Statistical Analysis

Quantitative data were expressed as the means ± standard deviation (SD). Statistical product and service solution (SPSS) 23.0 was used for statistical analysis. Data from two groups were analyzed with Independent-Samples *t*-test. GraphPad Prism 6.0 software was used to plot the graphical illustrations and curves. $P < 0.05$ was considered statistically significant.

Results

Preparation and Characterization of GVs, CTR-GVs, and ZD2-GVs

GVs were biosynthesized in *Halobacterium NRC-1* bacteria, and the isolation and purification procedure of GVs is shown in Figure 1a. TEM examination clearly showed that the GVs are monodisperse, with a rugby-ball-shaped structure (Figure 1b). Figure 1c shows that the FITC-labeled ZD2 or FITC-labeled control peptides were successfully conjugated to the surface of GVs, producing the absorption peaks of FITC at 488 nm. The ligation efficiency was calculated to be approximately 46% by quantifying the targeted and control peptides on the ligation by measuring the fluorescence intensity. The resulting ZD2-GVs and CTR-GVs had relatively uniform particle size distributions, similar to the plain GVs. The particle size of CTR-GVs and ZD2-GVs determined by a Zetasizer analyzer was 275.90 ± 5.69 nm and 267.73 ± 2.86 nm, respectively (Figure 1d), slightly larger than the plain GVs (246.13 ± 2.36 nm). The zeta potential of GVs, CTR-GVs and ZD2-GVs were −34.23 ± 2.71 mV, −38.43 ± 0.70 and −40.17 ± 1.21 mV, respectively (Figure 1e). No significant changes of zeta potentials were found in the peptide-modified GVs.

ED-B FN Expression in Murine Models of BC

The expression of ED-B FN was evaluated in normal liver tissues and tumor tissues. Immunofluorescence observed that tumor tissues highly expressed ED-B FN, and strong green fluorescence could be seen in the ECM. Normal liver tissue does not express ED-B FN, and no significant green fluorescence is seen in the ECM (Figure 2a). Western blot with the ED-B FN specific G4 antibody revealed the expression of 250 kDa bands consistent with the size of ED-B FN protein in tumor tissues and not in the normal liver tissue, indicating elevated ED-B FN expression in the tumors and no expression in the normal tissues and organs (Figure 2c).

Binding of ZD2-GVs to MB49 Cells

To validate the targeting binding capability of ZD2-GVs to MB49 tumor cells, we incubated FITC-labeled ZD2-GVs or CTR-GVs with the MB49 cells which have high level of expression of ED-B FN proteins. From Figure 3, we can see that FITC-labeled ZD2-GVs exhibited a significantly higher binding ability with MB49 cells than FITC-labeled CTR-GVs after 5 min incubation (Figure 3a). Notably, the pre-blocking with an excess of free ZD2 peptides greatly reduced the binding of ZD2-GVs to MB49 cells, indicating that ZD2-GVs can specifically bind with MB49 cells. Quantitative analysis showed that the mean fluorescence intensity from the cells appeared 13.19 ± 7.89 a.u., 85.98 ± 27.67 a.u., 21.91 ± 2.22 a.u. for CTR-GVs, ZD2-GVs, and ZD2-blocking group, respectively.

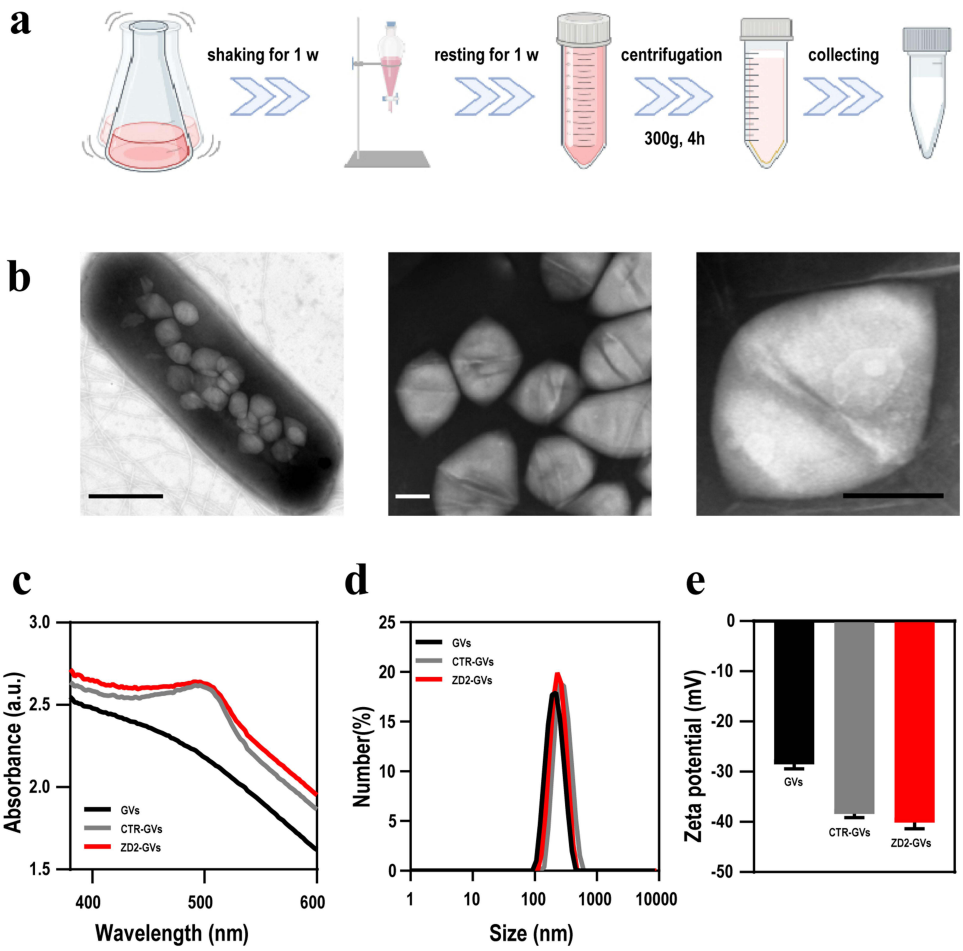

Figure 1 Preparation and characterization of GVs, CTR-GVs, and ZD2-GVs. (**a**) Isolation and purification of biosynthetic GVs; (**b**) TEM images of *Halobacterium NRC-1* (left) and isolated GVs (middle and right). The scale bars are 500 nm (left), 50 nm (middle), and 100 nm (right), respectively; (**c**) Absorbance spectra of GVs, CTR-GVs and ZD2-GVs; (**d**) Size distribution of GVs, CTR-GVs and ZD2-GVs; (**e**) Zeta potential of GVs, CTR-GVs and ZD2-GVs. Data of (**d** and **e**) represent the mean ± SD from 3 independent experiments.

In vitro Imaging Properties of ZD2-GVs

To evaluate the contrast imaging performance of ZD2-GVs, different concentrations of ZD2-GVs from OD_{500} 0.5 to 2.0 were imaged at the contrast mode. Figure 4a clearly shows that GVs, CTR-GVs and ZD2-GVs exhibited significantly enhanced contrast signals. The higher the concentrations of GVs, CTR-GVs and ZD2-GVs were, the stronger contrast signals of GVs, CTR-GVs and ZD2-GVs would be. The quantitative analysis of the average signal intensity revealed that GVs, CTR-GVs and ZD2-GVs at the same concentrations had comparable contrast signals (Figure 4b).

In vivo UMI

Next, we further evaluated the UMI capability of ZD2-GVs in tumor-bearing mice. GVs, CTR-GVs, and ZD2-GVs were intravenously injected in random order, with at least 30 min intervals. From the Figure 5b, we can see that there was no significant difference in peak signal intensities between GVs, CTR-GVs and ZD2-GVs in the MB49 tumors (25.99 ± 2.29 a.u. for GVs, 25.24 ± 0.42 a.u. for CTR-GVs, 34.48 ± 5.49 a.u. for ZD2-GVs). However, along with the time elongation, the signal intensity of the tumors received with ZD2-GVs was significantly higher than that of tumors received with GVs and CTR-GVs (Figure 5a and b), achieving 0.19 ± 0.03 a.u. for GVs, 2.63 ± 2.74 a.u. for CTR-GVs, and 22.83 ± 5.26 a.u. for ZD2-GVs group after 10 min. Figure 5b clearly shows a slower decay curve for ZD2-GVs group in comparison to GVs and CTR-GVs (n = 3). However, there was no significant difference in the contrast signal between the GVs group and the CTR-GVs groups. Approximately 3.60- or 8.77 - fold stronger contrast signals could be seen at 5 min and 10 min after injection

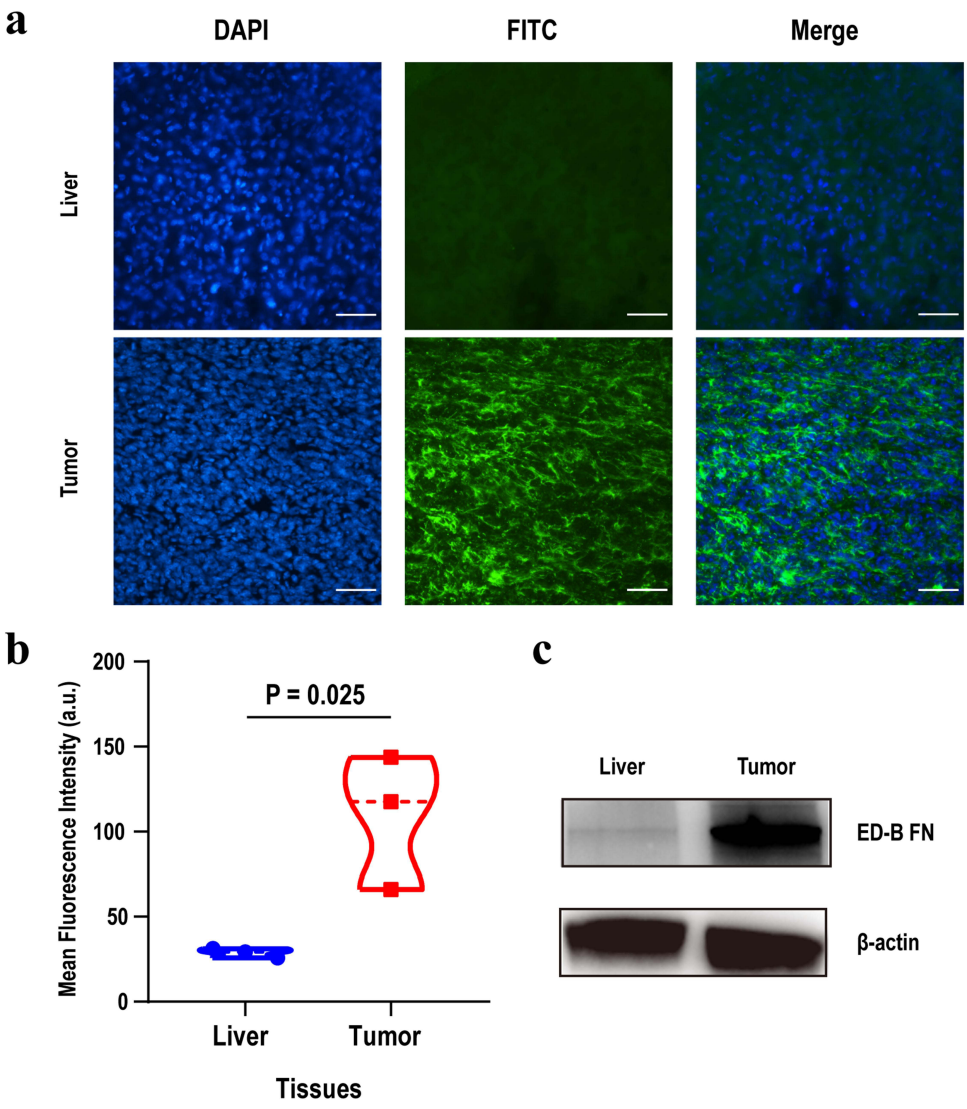

Figure 2 Immunofluorescence Staining and Western blots of ED-B FN in normal liver and tumor tissues. (**a**) Immunohistochemical staining of ED-B FN in liver and tumor tissues with and without G4 monoclonal antibody. Scale bar: 50 μm. (**b**) Quantification analysis of mean fluorescence intensity from (**a**). (**c**) Western blot analysis of the liver and tumor tissues protein lysates. Antibody G4 was used to characterize the ED-B FN expression, and expression of β-actin was used as the loading control.

than that of CTR-GVs group, confirming that ZD2-GVs had an excellent UMI performance in tumor-bearing mice (Figure 5c).

Distribution of GVs Tumor

To validate whether ZD2-GVs can be extravasated into the tumor matrix, FITC-labeled GVs, CTR-GVs, or ZD2-GVs at the same concentrations were simultaneously injected into the tail vein of the tumor-bearing mice. The tumors were sacrificed after 10 min, followed by section and observation with confocal microscope. From Figure 6a, we can see that numerous FITC-labeled ZD2-GVs was not only found in the vasculature but also in the extravascular spaces of the tumor (Figure 6a and b), which provides the strong evidence that the targeted GVs can extravasate from the vasculature and enter the tumor matrix space. Notably, significantly less non-targeted FITC-labeled GVs and FITC-labeled CTR-GVs could be observed in MB49 tumor.

In vitro and in vivo Toxicity Detection

The in vitro cytotoxicity was assessed by incubating different concentrations of GVs and ZD2-GVs with MB49 cells, followed by the CCK8 assay. Figure 7a and b clearly revealed that ZD2-GVs did not produce significant

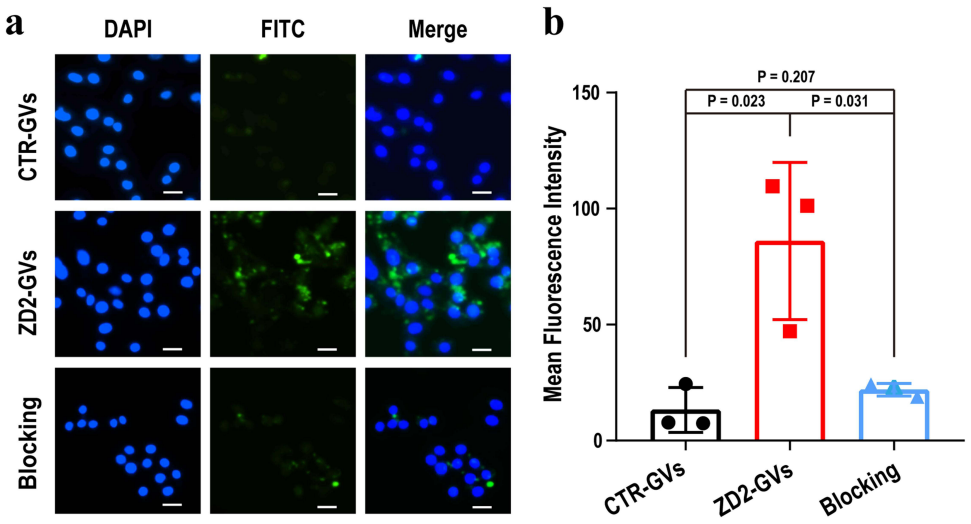

Figure 3 In vitro binding of ZD2-GVs to MB49 cells. (**a**) Representative fluorescent microscope images of MB49 cells incubated with FITC-labeled CTR-GVs, FITC-labeled ZD2-GVs and free ZD2 + FITC-labeled ZD2-GVs. Green stands for FITC-labeled GVs, and blue for cell nuclei stained with DAPI. Scale bar: 100 μm. (**b**) Quantification analysis of fluorescence intensities from (**a**). Data in (**b**) represent the mean ± SD from 3 independent experiments.

cytotoxicity to MB49 cells in comparison with GVs after 24 h or 48 h incubation. To confirm the biosafety of these GVs in vivo, the hematological data from healthy C57BL/6 mice injected intravenously with GVs or PBS on the first day and on the seventh day were analyzed, showing that the indicators of liver function (Alanine aminotransferase, ALT; Aspartate aminotransferase, AST) and renal function (Alkaline phosphatase, ALP; Blood urea nitrogen, BUN; Serum creatinine, CREA) fell within the normal range for both GVs and PBS groups (Figure 7c and d). H&E staining analysis did not find any pathological damage to heart, liver, spleen, lung, and kidneys in the mice received with GVs and ZD2-GVs (Figure 7e). All of these data indicated that GVs and ZD2-GVs were safe at the concentration of OD_{500} 3.0.

Discussion

Malignant tumors bring with serious threaten to the lives and health of patients. Early diagnosis plays an important role in detecting the tumorigenesis, progression and prognosis of tumors. Ultrasound is a noninvasive, widely available, low cost, real-time, and safe imaging modality in the clinical practice. With the advent of novel molecularly targeted ultrasound contrast agent, UMI technology makes great progresses, making it possibly get the early diagnosis of tumors. At present, the commonly used ultrasound contrast agent is based on the microscale bubbles and it is difficult for them to reach extravascular diseased tissues. Therefore, the development of NBs shows a promising application potential in the UMI. In recent years, biosynthetic GVs extracted from bacteria or algae have been developed. Shapiro et al first reported that protein-shelled, gas-filled GVs from *Halobacterium NRC-1* with widths of 45–250 nm, lengths of 100–600 nm, with biconical shapes, providing stable ultrasound contrast.[15] In our previous research, we have successfully demonstrated that biosynthetic GVs from *Halobacterium NRC-1* can be used for future molecular imaging and image-guided drug delivery.[9]

Among various biomarkers, FN containing ED-B domain is a promising candidate. Numerous evidences demonstrated that ED-B FN is associated with a number of cancer-related biological processes such as tumorigenesis, angiogenesis, and epithelial-to-mesenchymal transition.[26] Therefore, ED-B FN can be used as a specific marker for diagnosis of tumors. At present, although antibodies bind to ED-B FN, such as L-19 antibody[35] and different antibody variants (immunoglobulin G[36] [21777442], diabody,[37–39] mini-antibody/SIP,[40–42] and scFv),[43–45] have been

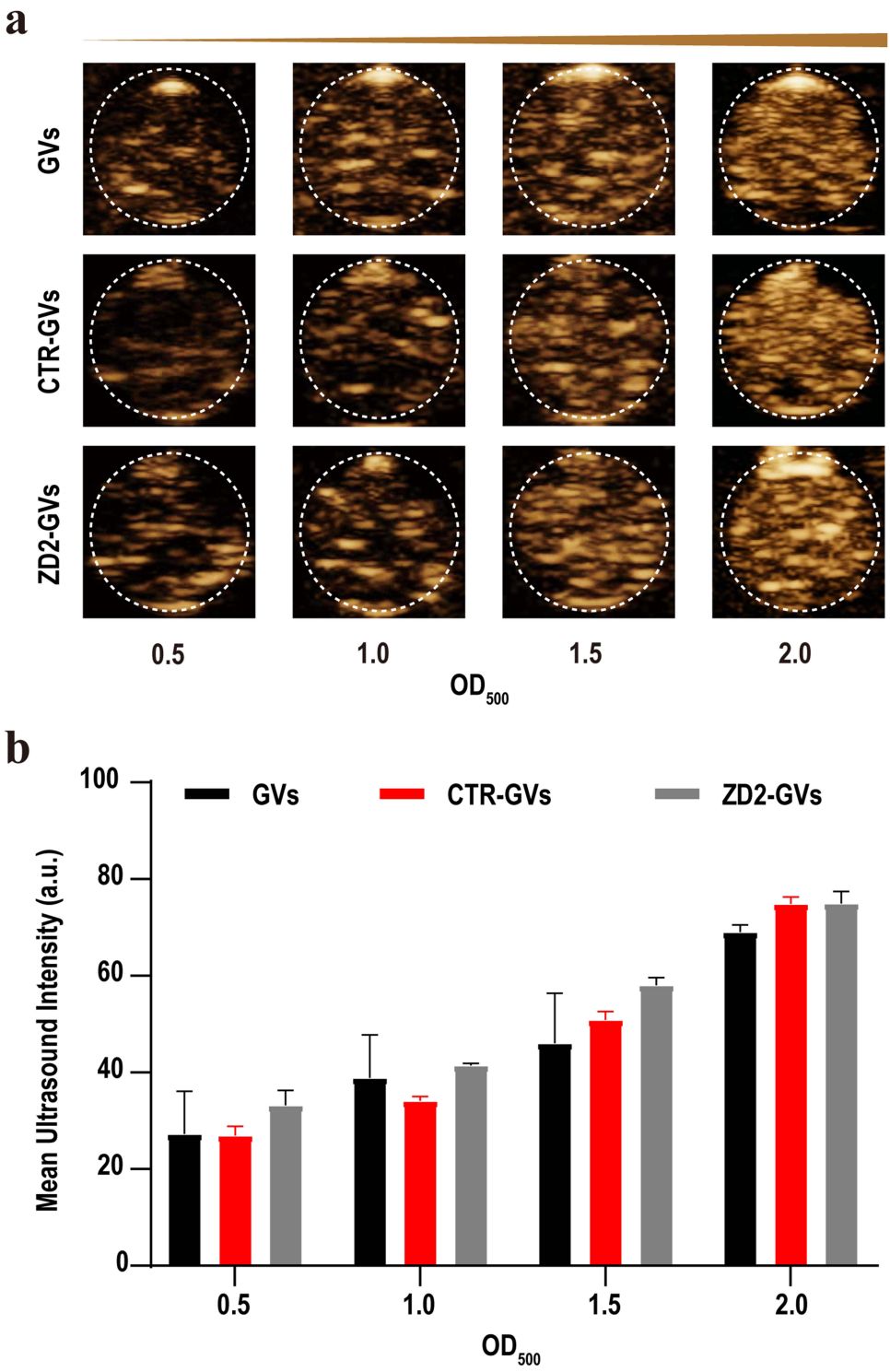

Figure 4 In vitro ultrasound contrast imaging of GVs, CTR-GVs, and ZD2-GVs. (**a**) Ultrasound contrast images of GVs, CTR-GVs, and ZD2-GVs at different concentrations (OD_{500} = 0.5 to 2.0). (**b**) Quantification analysis of mean ultrasound signal intensities from (**a**). Data represent the mean ± SD from 3 independent experiments.

developed and used, peptides have advantages over these antibodies due to their lack of immunogenicity and cost-effective methods of mass production.[26] In 2015, Han et al developed a peptide ZD2 (CTVRTSADC) that specifically binds to ED-B.[26] ZD2 is currently tested as a carrier for imaging purposes, such as for magnetic

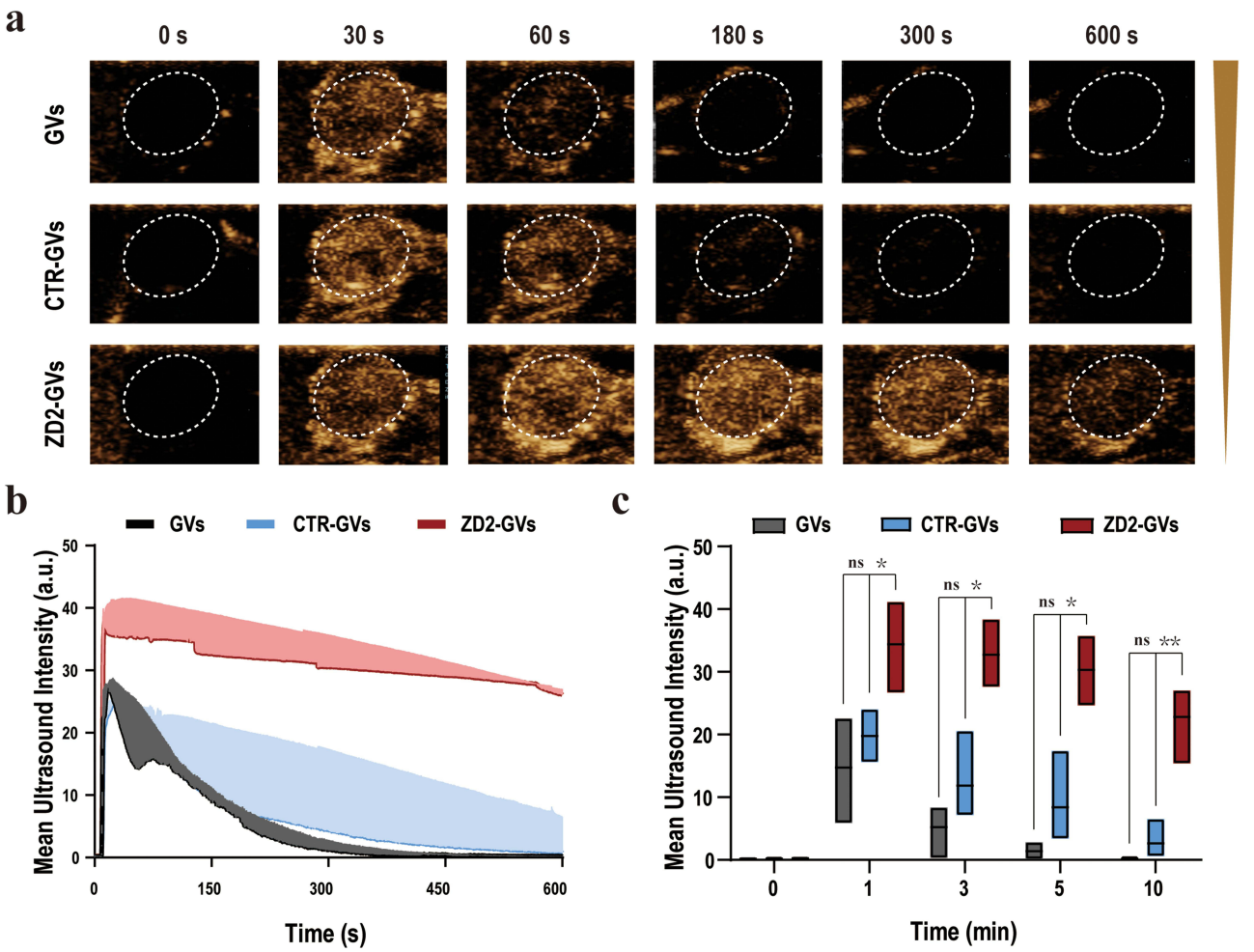

Figure 5 In vivo ultrasound molecular imaging of tumors. (**a**) Nonlinear contrast images of GVs, CTR-GVs, and ZD2-GVs (OD_{500} 3.0) at different time after intravenous injection. (**b**) Time-intensity curves of GVs, CTR-GVs and ZD2-GVs after intravenous injection. (**c**) The contrast signal intensities of tumors received with GVs, CTR-GVs, and GVs-ZD2 at 1 min, 3 min, 5 min, and 10 min. Data of (**b** and **c**) represent the mean ± SD from 3 independent experiments.*$p < 0.05$, **$p < 0.01$.

resonance imaging (MRI),[27–29] single-photon emission computed tomography (SPECT)[30] and magnetic resonance molecular imaging (MRMI).[28]

In this study, we prepared a kind of novel targeted NBs, ZD2-GVs, and explored their UMI capability of tumors. First, we found that ZD2-GVs have a small particle size, only with about 267 nm. It is especially beneficial for imaging of the tumor cell-surface biomarkers. Also, we confirmed that their targeting specificity to MB49 cells in vitro and their UMI performance in tumor-bearing mice. Just as shown in Figure 5, ZD2-GVs produced stronger contrast-enhanced signals and longer retention time in tumors in comparison to GVs and CTR-GVs, which indicates that more ZD2-GVs were bound to the tumor cells. Fluorescence immunohistochemistry valuated that FITC-labeled ZD2-GVs are distributed in the intravascular and extravascular spaces of BC tumors, suggesting that ZD2-GVs can penetrate the vascular system of tumor tissue and enter the interstitial space of the tumors. Thus, ZD2-GVs can function as a novel probe to image the expression of ED-B FN in the tumors, providing the tool for the early diagnosis of malignant tumors.

For the application of GVs, some important issues should be further addressed. In our study, we did not find that GVs were hazards to hosts or cells in the short term. However, it is noteworthy that GVs, composed of protein shells

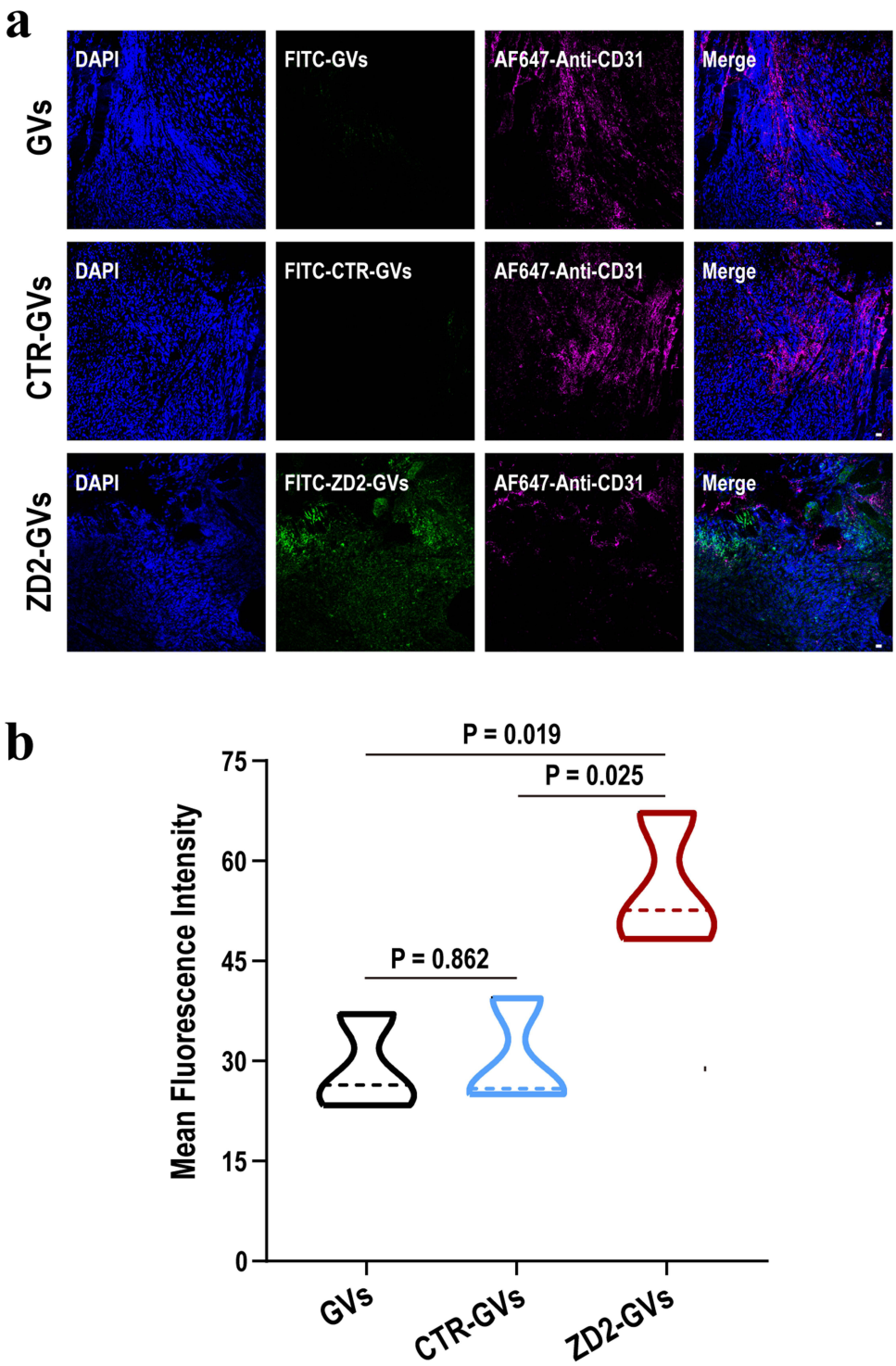

Figure 6 Histological analysis. (**a**) Representative fluorescence images of tumor sections from MB49 tumor-bearing mice injected with FITC-labeled GVs, FITC-labeled CTR-GVs, or FITC-labeled ZD2-GVs. Green stands for GVs, red for anti-CD31 antibody, and blue for cell nuclei stained with DAPI. Scale bar: 20 μm. (**b**) The mean fluorescence intensity of tumor sections at 3 random view fields. Data represent the mean ± SD from 3 independent experiments.

synthesized by bacteria, have a certain immunogenicity and can induce an immune response in mice. In our previous study,[46] PEG-GVs were successfully synthesized by PEG-coated GVs, and it was found that PEG-GVs greatly reduced the immunogenicity and reticuloendothelial system (RES) uptake, which provided a new idea for the clinical transformation of GVs in molecular imaging and disease diagnosis and treatment in the future.

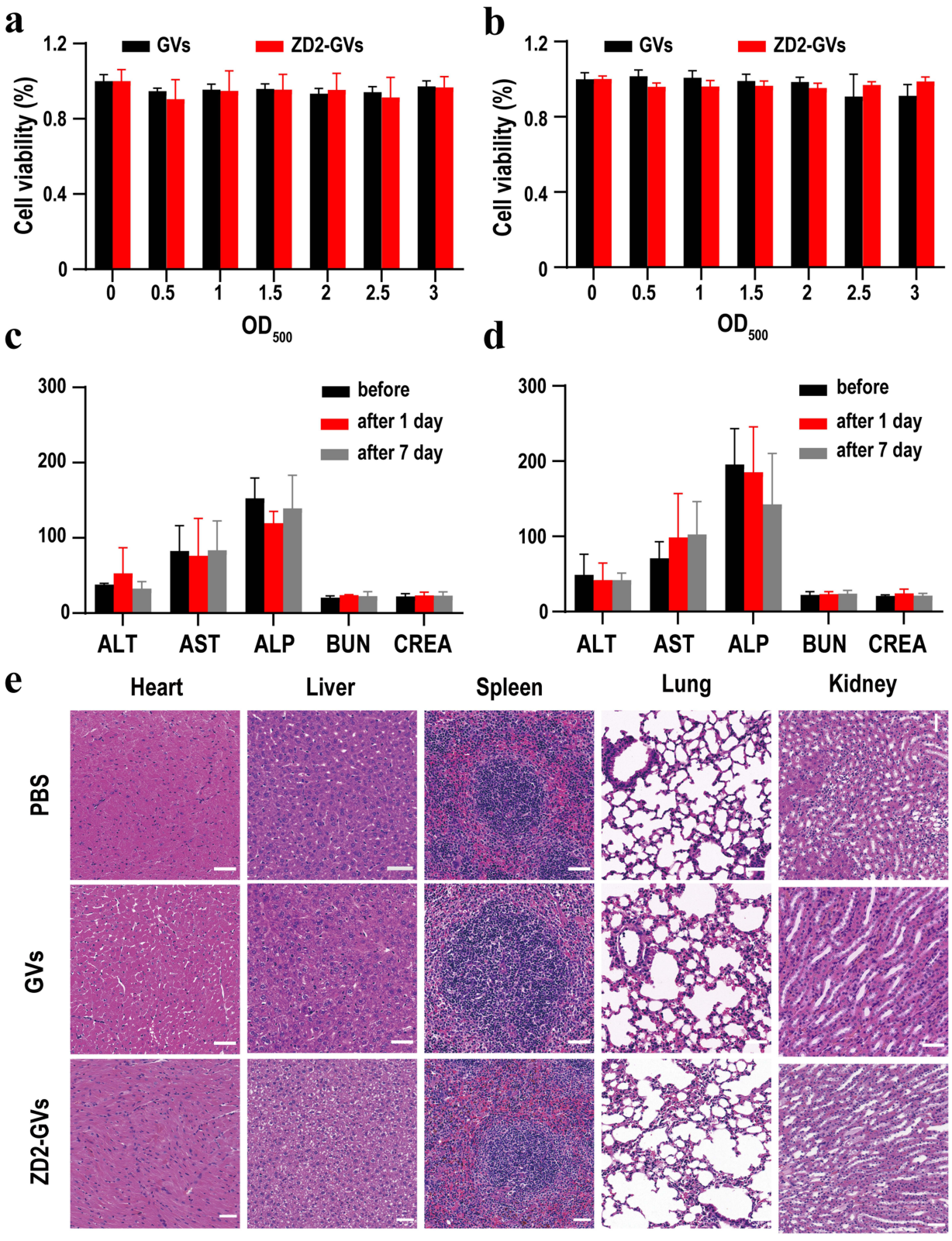

Figure 7 Biosafety analysis. (**a** and **b**) Viability of MB49 cells after treatment with GVs or ZD2-GVs at OD_{500} 0 to 3.0 for 24 h (**a**) and 48 h (**b**). (**c** and **d**) The levels of liver and kidney function indexes of mice received with the same volume of PBS (**c**) or GVs (**d**). The units of ALT, AST and ALP are UL^{-1}; the units of BUN and CREA are mg dl^{-1} and μmol L^{-1}, respectively. Injection of PBS with same volume was set as control groups. (**e**) Representative H&E sections of the main organs (heart, liver, spleen, lung, and kidney) from the mice received with PBS, GVs, or ZD2-GVs after 7 days. Scale bars: 50 μm. Data represent the mean ± SD from 3 independent experiments.

Conclusions

In summary, we developed ZD2-GVs as a novel acoustic probe, with small particle size and highly targeting capability to ED-B FN by using of biosynthetic GVs. Thanks to their nanoscale size, ZD2-GVs can penetrate tumor vasculature and specifically bind to tumor cells, making it possible to molecularly image the extravascular tumor parenchymal cells. Our study provides a promising tool for diagnosis of BC at the early stage.

Acknowledgments

This research was supported by the National Key R&D Program of China (2020YFA0908800), National Natural Science Foundation of China (No.82071929, No.81871376, No.82202158), Guangdong Innovation Platform of Translational Research for Cerebrovascular Diseases, and Shenzhen Science and Technology Innovation Committee (Grant Nos. JCYJ20190812171820731). Graphical abstract created with BioRender.com.

Disclosure

Yanan Feng, Yongsheng Hao, Weijian Song and Litao Sun report a patent 202310218086.4 pending to Fei Yan. The authors report no other conflicts of interest in this work.

References

1. Hernot S, Klibanov AL. Microbubbles in ultrasound-triggered drug and gene delivery. *Adv Drug Deliv Rev*. 2008;60(10):1153–1166. doi:10.1016/j.addr.2008.03.005
2. Hussain T, Nguyen QT. Molecular imaging for cancer diagnosis and surgery. *Adv Drug Deliv Rev*. 2014;66:90–100. doi:10.1016/j.addr.2013.09.007
3. Abou-Elkacem L, Bachawal SV, Willmann JK. Ultrasound molecular imaging: moving toward clinical translation. *Eur J Radiol*. 2015;84(9):1685–1693. doi:10.1016/j.ejrad.2015.03.016
4. van Rooij T, Daeichin V, Skachkov I, de Jong N, Kooiman K. Targeted ultrasound contrast agents for ultrasound molecular imaging and therapy. *Int J Hyperthermia*. 2015;31(2):90–106. doi:10.3109/02656736.2014.997809
5. Xing Z, Wang J, Ke H, et al. The fabrication of novel nanobubble ultrasound contrast agent for potential tumor imaging. *Nanotechnology*. 2010;21(14):145607. doi:10.1088/0957-4484/21/14/145607
6. Marxer EE, Brussler J, Becker A, et al. Development and characterization of new nanoscaled ultrasound active lipid dispersions as contrast agents. *Eur J Pharm Biopharm*. 2011;77(3):430–437. doi:10.1016/j.ejpb.2010.12.007
7. Kim M, Lee JH, Kim SE, Kang SS, Tae G. Nanosized ultrasound enhanced-contrast agent for in vivo tumor imaging via intravenous injection. *ACS Appl Mater Interfaces*. 2016;8(13):8409–8418. doi:10.1021/acsami.6b02115
8. Zhou QL, Chen ZY, Wang YX, Yang F, Lin Y, Liao YY. Ultrasound-mediated local drug and gene delivery using nanocarriers. *Biomed Res Int*. 2014;2014:963891. doi:10.1155/2014/963891
9. Wei M, Lai M, Zhang J, Pei X, Yan F. Biosynthetic gas vesicles from halobacteria NRC-1: a potential ultrasound contrast agent for tumor imaging. *Pharmaceutics*. 2022;14(6):1198. doi:10.3390/pharmaceutics14061198
10. Hao Y, Li Z, Luo J, Li L, Yan F. Ultrasound molecular imaging of epithelial mesenchymal transition for evaluating tumor metastatic potential via targeted biosynthetic gas vesicles. *Small*. 2023;19(21):e2207940. doi:10.1002/smll.202207940
11. Pfeifer F. Distribution, formation and regulation of gas vesicles. *Nat Rev Microbiol*. 2012;10(10):705–715. doi:10.1038/nrmicro2834
12. Piraner DI, Farhadi A, Davis HC, et al. Going deeper: biomolecular tools for acoustic and magnetic imaging and control of cellular function. *Biochemistry*. 2017;56(39):5202–5209. doi:10.1021/acs.biochem.7b00443
13. Bourdeau RW, Lee-Gosselin A, Lakshmanan A, et al. Acoustic reporter genes for noninvasive imaging of microorganisms in mammalian hosts. *Nature*. 2018;553(7686):86–90. doi:10.1038/nature25021
14. Pfeifer F. Haloarchaea and the formation of gas vesicles. *Life*. 2015;5(1):385–402. doi:10.3390/life5010385
15. Shapiro MG, Goodwill PW, Neogy A, et al. Biogenic gas nanostructures as ultrasonic molecular reporters. *Nat Nanotechnol*. 2014;9(4):311–316. doi:10.1038/nnano.2014.32
16. Walsby AE. Gas vesicles. *Microbiol Rev*. 1994;58(1):94–144. doi:10.1128/mr.58.1.94-144.1994
17. Zhou Z, Lu ZR. Molecular imaging of the tumor microenvironment. *Adv Drug Deliv Rev*. 2017;113:24–48. doi:10.1016/j.addr.2016.07.012
18. Park J, Schwarzbauer JE. Mammary epithelial cell interactions with fibronectin stimulate epithelial-mesenchymal transition. *Oncogene*. 2014;33(13):1649–1657. doi:10.1038/onc.2013.118
19. Alisson-Silva F, Freire-de-lima L, Donadio JL, et al. Increase of O-glycosylated oncofetal fibronectin in high glucose-induced epithelial-mesenchymal transition of cultured human epithelial cells. *PLoS One*. 2013;8(4):e60471. doi:10.1371/journal.pone.0060471
20. Borsi L, Carnemolla B, Neri D, Zardi L. Use of human recombinant antibodies to the marker of angiogenesis ed-b in cancer therapy. *Tumori*. 2001;87(6):S8–10. doi:10.1177/030089160108700629
21. Hajitou A, Pasqualini R, Arap W. Vascular targeting: recent advances and therapeutic perspectives. *Trends Cardiovasc Med*. 2006;16(3):80–88. doi:10.1016/j.tcm.2006.01.003
22. Mani SA, Guo W, Liao MJ, et al. The epithelial-mesenchymal transition generates cells with properties of stem cells. *Cell*. 2008;133(4):704–715. doi:10.1016/j.cell.2008.03.027
23. Han Z, Lu ZR. Targeting fibronectin for cancer imaging and therapy. *J Mater Chem B*. 2017;5(4):639–654. doi:10.1039/C6TB02008A
24. Qiao P, Ayat NR, Vaidya A, et al. Magnetic resonance molecular imaging of extradomain B fibronectin improves imaging of pancreatic cancer tumor xenografts. *Front Oncol*. 2020;10:586727. doi:10.3389/fonc.2020.586727

25. Hall RC, Ayat NR, Qiao PL, et al. Preclinical assessment of the effectiveness of magnetic resonance molecular imaging of extradomain-B fibronectin for detection and characterization of oral cancer. *Mol Imaging Biol*. 2020;22(6):1532–1542. doi:10.1007/s11307-020-01524-6
26. Han Z, Zhou Z, Shi X, et al. EDB fibronectin specific peptide for prostate cancer targeting. *Bioconjug Chem*. 2015;26(5):830–838. doi:10.1021/acs.bioconjchem.5b00178
27. Ayat NR, Qin JC, Cheng H, et al. Optimization of ZD2 peptide targeted gd(HP-DO3A) for detection and risk-stratification of prostate cancer with MRI. *ACS Med Chem Lett*. 2018;9(7):730–735. doi:10.1021/acsmedchemlett.8b00172
28. Ayat NR, Vaidya A, Yeung GA, et al. Effective MR molecular imaging of triple negative breast cancer with an EDB-fibronectin-specific contrast agent at reduced doses. *Front Oncol*. 2019;9:1351. doi:10.3389/fonc.2019.01351
29. Han Z, Li Y, Roelle S, et al. Targeted contrast agent specific to an oncoprotein in tumor microenvironment with the potential for detection and risk stratification of prostate cancer with MRI. *Bioconjug Chem*. 2017;28(4):1031–1040. doi:10.1021/acs.bioconjchem.6b00719
30. Ye XX, Zhao YY, Wang Q, et al. EDB fibronectin-specific SPECT probe (99m)Tc-HYNIC-ZD2 for breast cancer detection. *ACS Omega*. 2017;2(6):2459–2468. doi:10.1021/acsomega.7b00226
31. Han Z, Wu X, Roelle S, Chen C, Schiemann WP, Lu ZR. Author correction: targeted gadofullerene for sensitive magnetic resonance imaging and risk-stratification of breast cancer. *Nat Commun*. 2018;9(1):153. doi:10.1038/s41467-017-02302-9
32. Yao AI, Facciotti MT. Regulatory multidimensionality of gas vesicle biogenesis in Halobacterium salinarum NRC-1. *Archaea*. 2011;2011:716456. doi:10.1155/2011/716456
33. Lakshmanan A, Lu GJ, Farhadi A, et al. Preparation of biogenic gas vesicle nanostructures for use as contrast agents for ultrasound and MRI. *Nat Protoc*. 2017;12(10):2050–2080. doi:10.1038/nprot.2017.081
34. Lieverse RIY, Marcus D, van der Wiel AMA, et al. Human fibronectin extra domain B as a biomarker for targeted therapy in cancer. *Mol Oncol*. 2020;14(7):1555–1568. doi:10.1002/1878-0261.12705
35. Pini A, Viti F, Santucci A, et al. Design and use of a phage display library. Human antibodies with subnanomolar affinity against a marker of angiogenesis eluted from a two-dimensional gel. *J Biol Chem*. 1998;273(34):21769–21776. doi:10.1074/jbc.273.34.21769
36. Mohlmann S, Bringmann P, Greven S, Harrenga A. Site-specific modification of ED-B-targeting antibody using intein-fusion technology. *BMC Biotechnol*. 2011;11:76. doi:10.1186/1472-6750-11-76
37. Danielli R, Patuzzo R, Di Giacomo AM, et al. Intralesional administration of L19-IL2/L19-TNF in stage III or stage IVM1a melanoma patients: results of a Phase II study. *Cancer Immunol Immunother*. 2015;64(8):999–1009. doi:10.1007/s00262-015-1704-6
38. Rekers NH, Olivo Pimentel V, Yaromina A, et al. The immunocytokine L19-IL2: an interplay between radiotherapy and long-lasting systemic anti-tumour immune responses. *Oncoimmunology*. 2018;7(4):e1414119. doi:10.1080/2162402X.2017.1414119
39. Zegers CM, Rekers NH, Quaden DH, et al. Radiotherapy combined with the immunocytokine L19-IL2 provides long-lasting antitumor effects. *Clin Cancer Res*. 2015;21(5):1151–1160. doi:10.1158/1078-0432.CCR-14-2676
40. Borsi L, Balza E, Bestagno M, et al. Selective targeting of tumoral vasculature: comparison of different formats of an antibody (L19) to the ED-B domain of fibronectin. *Int J Cancer*. 2002;102(1):75–85. doi:10.1002/ijc.10662
41. Steiner M, Neri D. Antibody-radionuclide conjugates for cancer therapy: historical considerations and new trends. *Clin Cancer Res*. 2011;17(20):6406–6416. doi:10.1158/1078-0432.CCR-11-0483
42. Tijink BM, Perk LR, Budde M, et al. (124)I-L19-SIP for immuno-PET imaging of tumour vasculature and guidance of (131)I-L19-SIP radioimmunotherapy. *Eur J Nucl Med Mol Imaging*. 2009;36(8):1235–1244. doi:10.1007/s00259-009-1096-y
43. Menrad A, Menssen HD. ED-B fibronectin as a target for antibody-based cancer treatments. *Expert Opin Ther Targets*. 2005;9(3):491–500. doi:10.1517/14728222.9.3.491
44. Ventura E, Balza E, Borsi L, et al. Selective targeted delivery of the TNF-alpha receptor p75 and uteroglobin to the vasculature of inflamed tissues: a preliminary report. *BMC Biotechnol*. 2011;11:104. doi:10.1186/1472-6750-11-104
45. Viti F, Tarli L, Giovannoni L, Zardi L, Neri D. Increased binding affinity and valence of recombinant antibody fragments lead to improved targeting of tumoral angiogenesis. *Cancer Res*. 1999;59(2):347–352.
46. Wang Y, Fu M, Yang Y, et al. Modification of PEG reduces the immunogenicity of biosynthetic gas vesicles. *Front Bioeng Biotechnol*. 2023;11:1128268. doi:10.3389/fbioe.2023.1128268